

Uniformity of foreground Galactic neutral Hydrogen over cooling flow clusters

D. G. Barnes^{1*} and P. E. J. Nulsen²

¹*School of Physics, University of Melbourne, Vic 3010, Australia*

²*Engineering Physics, University of Wollongong, NSW 2522, Australia*

2002 July 9

ABSTRACT

Radio maps at 21 cm of foreground neutral hydrogen over three cooling flow clusters of galaxies show that the foreground gas is uniform on scales from $\sim 1 - 10$ arcmin. Five sigma limits on fluctuations in the foreground column density for Abell 3581, Sersic 159-03 and Abell 2597 are 6.2×10^{19} , 7.8×10^{19} and $4.3 \times 10^{19} \text{ cm}^{-2}$, or 14, 43 and 17 percent of the mean foreground column density in the region of the system, respectively. Fluctuations in the column density of neutral gas in the Galaxy are unlikely to account for any excesses of photoelectric absorption in these or other cooling flow clusters. Fluctuations in the foreground neutral gas on arcminute scales are also unlikely to be the cause of excess EUV and soft X-ray emission from clusters.

Key words: ISM: structure – galaxies: cluster: individual: A3581, A2597, Sersic 159-03 – cooling flows – intergalactic medium – X-rays: galaxies: clusters

1 INTRODUCTION

Data from *Chandra* and *XMM-Newton* have caused radical revisions to the X-ray view of cooling flows in clusters of galaxies (Fabian 1994). Where data from X-ray missions such as *ROSAT* and *ASCA* were interpreted as showing that substantially more than $100 M_{\odot} \text{ yr}^{-1}$ of cooled gas is being deposited in the central regions of many clusters (White, Jones & Fabian 1997; Peres et al. 1998; Allen et al. 2001), *Chandra* and *XMM-Newton* data are inconsistent with such high cooling rates (e.g. David et al. 2001), and show little spectroscopic evidence

* E-mail: dbarnes@isis.ph.unimelb.edu.au

for gas cooling below temperatures of about 1 keV (e.g. Peterson et al. 2001; Tamura et al. 2001).

The cooling time of the gas at the centre of a cooling flow cluster is typically only a few times 10^8 yr, so that substantial heat input is required to prevent large amounts of gas from cooling below 1 keV. The rapidly growing list of cavities found in the X-ray emitting gas associated with radio lobes emanating from the nucleus of the central galaxy (e.g. McNamara et al. 2000; Fabian et al. 2000; Blanton et al. 2001) suggests strongly that radio outbursts from the active nucleus of the central galaxy provide the required heating (Churazov et al. 2002; Nulsen et al. 2002).

Many issues remain to be settled in the emerging picture of cluster cooling flows (e.g. Fabian et al. 2001). In particular, the presence of cool gas in a wide variety of forms (e.g. Crawford et al. 1999; Donahue et al. 2000; Edge 2001; Edge et al. 2002) and star formation (e.g. Johnstone, Fabian & Nulsen 1987; McNamara & O’Connell 1992; Crawford et al. 1999; Mittaz et al. 2001) in many of these systems indicates that some of the X-ray emitting intracluster gas does cool to low temperatures. This is supported by the detection of some X-ray emitting gas below 1 keV in at least one system (Kaastra et al. 2001). However, it is yet to be determined how the cooled gas arises. It might be deposited in brief episodes every few times 10^8 yr, as the central gas radiates the last of its thermal energy, cools to low temperatures and triggers a nuclear outburst that chokes off further cooling. Alternatively, it may be deposited as a continuous thermally unstable trickle (e.g. Oegerle et al. 2001). It has also been proposed that at least some of the cool gas did not originate as intracluster gas, but was brought to the cluster centre with infalling galaxies (McNamara 1997). As well, the state of the bulk of the cool gas at the centres of cooling flows is disputed (Ferland, Fabian & Johnstone 1994; Voit & Donahue 1995).

In this paper we discuss maps of Galactic foreground HI emission over cooling flow clusters. This work was originally prompted by measurements of large excess photoelectric absorption in cooling flow clusters (White et al. 1991; Allen & Fabian 1997; Allen 2000), implying very large reservoirs of cooled gas within them. The aim was to determine if arcminute scale fluctuations in foreground HI column density could account for the excess absorption (David, Jones & Forman 1996 proposed that variations in foreground dust column density could have this effect). However, *Chandra* and *XMM-Newton* observations now suggest that the excess photoelectric absorption was largely an artifact of models in which large quantities of gas were assumed to cool from the ambient temperature of the intracluster

medium to well below 1 keV. Nevertheless, photoelectric absorption by the cool gas remains an important channel for information about its quantity and state, and for this purpose it is important to be able separate the effects of foreground absorption.

A number of authors have reported extreme ultraviolet (EUV) and soft X-ray excesses in clusters of galaxies (e.g. Lieu et al. 1996; Kaastra et al. 1999; Bowyer, Berghöfer & Korpela 1999; Bonamente, Lieu & Mittaz 2001; but see Berghöfer & Bowyer 2002). Such an excess could be due to inverse Compton scattering of the microwave background by a non-thermal particle population, but then the minimum particle pressure required in the cluster Sersic 159-03 would exceed the thermal pressure of the hot gas (Bonamente et al. 2001). In order to maintain hydrostatic equilibrium, that would imply at least doubling the cluster mass. Alternatively, the soft excess in Sersic 159-03 may be due to gas that is cooler than the hot intracluster medium, but then the total mass of cool gas would be comparable to that of the hot gas (Bonamente et al. 2001). This presents the problem that the huge mass of cool gas cannot be stably supported by hydrostatic pressure. Measurements of EUV and soft X-ray emission from extragalactic sources are sensitive to correction for foreground photoelectric absorption. Arabadjis & Bregman (1999) have argued on this basis that the evidence for soft emission from a number of clusters is weak. Krick, Arabadjis & Bregman (2000) have argued further that arcminute scale holes in the foreground absorption might account for at least part of the soft excess. So, the uniformity of foreground HI emission is also of interest for clusters showing EUV and soft X-ray excesses.

In section 2 we describe the observations and data reduction. Our main result is that there is no evidence for arcmin scale structure in the foreground HI emitting gas. In section 3 we discuss the limits we can place on variation of foreground HI for each case. For the purpose of obtaining scales, we assume a flat Λ CDM cosmology, with $H_0 = 70 \text{ km s}^{-1} \text{ Mpc}^{-1}$ and $\Omega_m = 0.3$ throughout the paper.

2 OBSERVATIONS AND DATA REDUCTION

We selected the cooling flow clusters A3581, A2597 and Sersic 159-03 because they have shown photoelectric absorption well in excess of that expected due to foreground gas (Allen & Fabian 1997; Johnstone, Fabian & Taylor 1998). As already noted, Sersic 159-03 is also reported as having the greatest known soft X-ray excess (Bonamente et al. 2001). Pertinent details of the clusters are given in Table 1.

Table 1. Cooling flow clusters: observing and image parameters.

Cluster	Position		Redshift	Integration time ^a (hr)	Natural weight		Uniform weight	
	RA (J2000)	Dec			Image beam ^b (arcsec ²)	RMS noise ^c (mJy beam ⁻¹)	Image beam (arcsec ²)	RMS noise (mJy beam ⁻¹)
Abell 3581	14 07	−27 01	0.023	8.6	139 × 51	2.2	85 × 42	3.5
Sersic 159-03	23 14	−42 43	0.058	10.3	101 × 77	2.9	60 × 50	5.0
Abell 2597	23 25	−12 06	0.085	11.7	396 × 59	2.9	199 × 43	4.4

^a Total effective integration time after data editing.

^b The dimensions of a Gaussian fitted to the synthesized beam are given; they are mildly sensitive to the image pixel size.

^c The square root of the pixel-to-pixel variance is given, calculated for regions of the the image volumes devoid of sources.

To image the Galactic foreground HI which might be screening the cooling flows at the centres of the clusters, we have used the Australia Telescope Compact Array (ATCA) in two moderately compact configurations: 375 and 750A. The ATCA is an unfilled-aperture, rotation synthesis interferometer, and as such measures only a finite set of spatial (angular) components of the source distribution. In particular, the minimum baseline within the array sets the size of the largest well-imaged structure, which for the configurations used is ~ 10 arcmin. Features (ie. emission, absorption) in the source distribution larger than this are largely invisible to the telescope. To a good approximation then, our observations will produce images of the “fine structure” in the foreground HI, that is, the modulation in the HI above some pedestal value which varies slowly across the sky and can only be measured by a filled-aperture (ie. single-dish) radio telescope.

Observations were acquired using the 375 configuration on 1996 December 4 and 7, and the 750A configuration on 1998 May 9, 10 and 12. Observations of A3581 were made only with the 750A configuration. The half-power beam width of an ATCA antenna at wavelength 21 cm is 33 arcmin, and this sets the size of the field imaged by a single pointing of the array; beyond ~ 16 arcmin from the field centre the sensitivity falls off rapidly. The image resolution within the 33 arcmin field is determined by the maximum antenna–antenna baseline within the array, which for all fields was 735 m, corresponding to a theoretical resolution of ~ 60 arcsec in the R.A. direction. Because the ATCA is an East-West array and uses the Earth’s rotation to synthesize a planar interferometer, the resolution in the Dec direction is elongated by a factor $|\sin^{-1}\delta|$ for observations at Dec δ ; this effect is particularly severe for A2597 at $\delta = -12^\circ 06'$.

To image Galactic gas, the ATCA receiver chain and correlator were programmed to record XX and YY correlations between all telescope pairings over a bandwidth of 8 MHz, centred on 1420 MHz. The band was divided into 1024 raw channels, yielding redshifted

spectral channels of width 1.65 km s^{-1} extending from -760 to $+930 \text{ km s}^{-1}$ in the frame of the observations.¹ The primary calibrator 1934–638 was observed for absolute flux calibration (Reynolds 1994) at the start of each observing period, and (weaker) secondary calibrators were observed regularly during each observation to enable the determination of time-dependent bandpass calibration solutions.

The data were edited, calibrated and imaged in the radio interferometry data reduction package MIRIAD. Some editing of the visibility data for the program sources was necessary where on-line flagging had not been aggressive enough, and where transient interference and/or system faults were evident. Any continuum emission present in the visibility data was removed by fitting and subtracting a first-order polynomial from every visibility spectrum; the fit was made to the outer channels in the band to avoid contamination by Galactic HI line emission. Radio continuum images at 1420 MHz were made using the continuum fit data, and yielded three sources with peak flux exceeding 10 mJy in the A2597 and Sersic 159-03 fields, and four in the A3581 field. The clusters themselves were detected at the following peak fluxes: A3581: $0.40 \pm 0.02 \text{ Jy}$; Sersic 159-03: $0.21 \pm 0.02 \text{ Jy}$; and A2597: $1.74 \pm 0.05 \text{ Jy}$.

Images were produced by gridding and Fourier-inverting the continuum-subtracted visibility data, averaging two raw channels at a time and eliminating the (noisier) band edges, to produce images having 200 planes (channels) of width 3.31 km s^{-1} , occupying the radial velocity domain $-331 < V_{\text{LSRK}} < +331 \text{ km s}^{-1}$ measured in the local standard of rest (kinematic) frame. Image pixel sizes were selected to sub-sample the synthesized beam by a factor of ~ 3 in each direction. We used two standard schemes to weight the visibility data during the inversion: uniform weighting which assigns equal weight to all visibilities and produces images of high angular resolution at the cost of increased noise; and natural weighting, which favours visibility data from the shorter baselines and produces images of lower angular resolution but significantly lower noise. The total effective integration time, image beam dimensions and image noise levels for the observed fields are given in Table 1. The image noise levels are close to theoretical. The spatial correlation scale in the images is well described by a two-dimensional Gaussian having the dimensions listed in Table 1 (i.e. the synthesized beam, typically three pixels across). Along the spectral axis, the images are $\gtrsim 90$ per cent uncorrelated.

Table 1 lists image noise values for regions of each image which are free of obvious HI

¹ Note that the velocity *resolution* is 1.21 times the channel width.

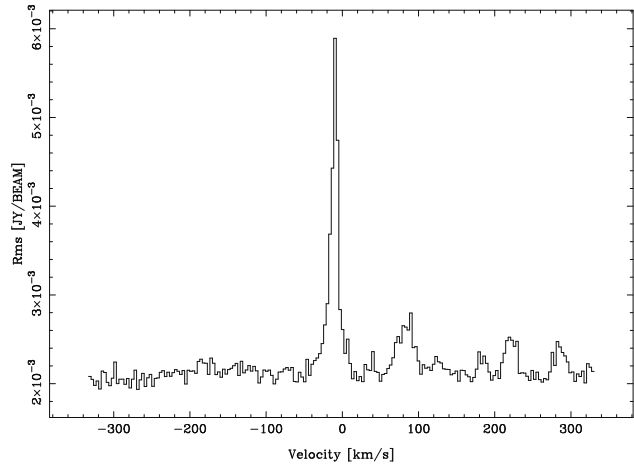


Figure 1. RMS pixel variation per channel for A3581. Features at -10 and 90 km s^{-1} are sidelobe artefacts of narrow linewidth sources well away from the primary beam of the telescope. The features at 220 and 290 km s^{-1} are locations of genuinely increased noise probably due to narrowband interference.

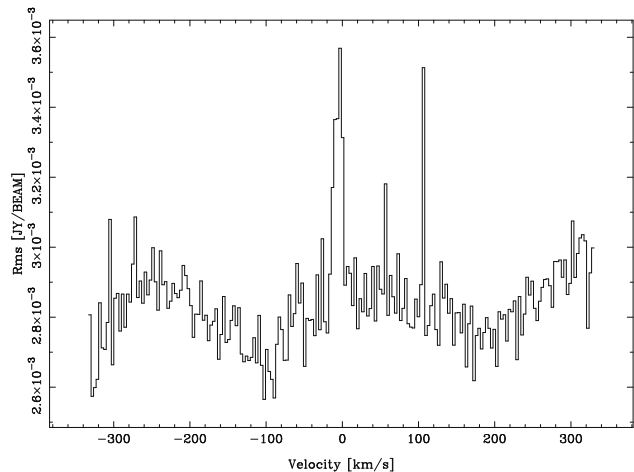


Figure 2. RMS pixel variation per channel for Sersic 159-03. The slightly elevated noise level near 0 km s^{-1} is due to a faint grating pattern across the channel maps, probably arising from internal interference.

emission sources. To assess any variation in image noise across the field, we produced maps of the RMS pixel value along each sky pixel in the non-primary-beam-corrected image cubes. Towards each cluster, the RMS varied by less than 10 per cent from the value listed in Table 1 over the sky. To assess any variation in image noise through the frequency space of the observations, we produced a spectrum of the RMS pixel variation per channel; the RMS noise spectra are reproduced in Figures 1–3 for the naturally-weighted images. The spectra again show very little variation throughout the frequency domain, except for a few features which we now discuss.

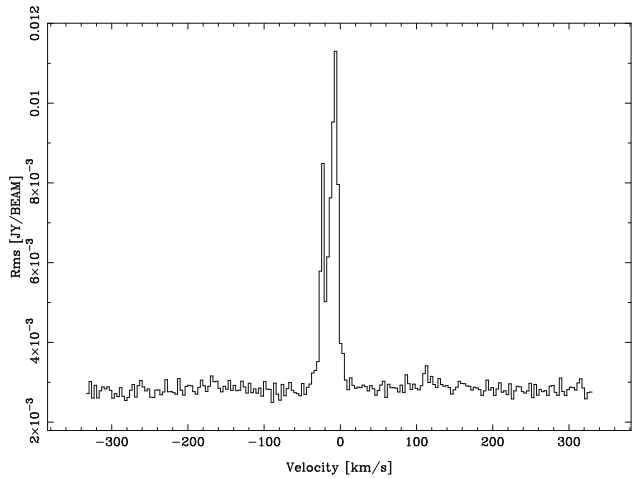


Figure 3. RMS pixel variation per channel for A2597.

A3581. The features at -10 and $+90$ km s^{-1} in the RMS spectrum towards A3581 (Figure 1) are due to sidelobes of strong, narrow linewidth and point-like sources well outside the primary beam of the telescope. Careful inspection of the calibrator spectra rules out the chance that these are artefacts introduced by Galactic absorption towards the secondary calibrator source, and consequently we believe them to be real “hot spots” in the Galactic HI column. These features are similar to the signature this project aims to find, but are well away (> 40 arcmin) from the line-of-sight to the cluster, and are simply bright enough to be detected in the sidelobes of the telescope. The features at 220 and 290 km s^{-1} are channels having genuinely increased noise due to narrowband interference, some of which has been flagged. Apart from these features, the noise in this field is steady at 2.2 mJy beam^{-1} .

Sersic 159-03. This field exhibits slightly elevated noise near 0 km s^{-1} , where a grating pattern is evident in the channel maps. This is either due to interference (probably internal to the system) which is too weak to identify and flag in the raw visibility data, or to a strong, narrow source passing through a distant sidelobe of the telescope. It is certainly not characteristic of local emission (or absorption) along the line of sight to the cluster. It only marginally affects our ability to detect a foreground excess of the magnitude required (see below). The noise in this field is generally less than 2.9 mJy beam^{-1} .

A2597. The HI emission in the A2597 field is complex and difficult to interpret. Figure 3 shows substantial “pollution” extending from -30 to 0 km s^{-1} , of an otherwise flat noise profile. In Figure 4 we present individual channel maps covering this velocity range, selected from the naturally-weighted image. In these unCLEANed maps, sources are convolved with

Table 2. Limits on arcmin scale variations in foreground neutral hydrogen column density

Cluster	N_{HI}		Channels ^a	Natural weight			Uniform weight		
	S92 ^b	HB97 ^c		ΔN_{HI} (10^{20} cm^{-2})			ΔN_{HI} (10^{20} cm^{-2})		
	$(10^{20} \text{ cm}^{-2})$			summed ^d	averaged ^e	measured^f	summed	averaged	measured
Abell 3581	4.5	4.1	36	2.0	0.34	0.62	6.4	1.1	1.2
Sersic 159-03	1.8	n/a	64	4.4	0.55	0.78	17	2.1	2.5
Abell 2597	2.5	2.5	48	1.1	0.16	0.43	5.1	0.74	0.66

^a number of 3.3 km s^{-1} channels with significant foreground emission in HIPASS data.

^b Stark et al. (1992), ~ 2 degree beam

^c Hartmann & Burton (1997), ~ 35 arcmin beam

^d 5σ noise per channel summed over the channels with foreground emission.

^e summed 5σ noise divided by the square root of the number of contributing channels.

^f image-plane RMS in moment map generated over HIPASS-determined channels

the synthesized beam and so even a simple source distribution on the sky could produce the bulk of the observed pattern; elliptical sidelobes are particularly evident in the bottom-left and top-right panels of Figure 4. However there are also fainter grating patterns, most obvious in the second and third panels, but possibly extant in all the maps. Grating patterns are generally the result of a fixed interference source present for some or all of the observations and despite our efforts, it has not been possible to find and eliminate the offending data in this case.

In Figure 5, we show the result of iteratively deconvolving the channel maps of Figure 4 and restoring the images with a Gaussian beam fitted to the synthesized beam, using the MIRIAD tasks CLEAN and RESTOR. The resultant maps, aside from the genuine hot-spot in the top-right panel, and possibly those in the bottom-left panel (none of which are aligned with the cluster cooling flow), appear to contain a semi-regular array of sources. It seems far more likely that these are artefacts where multiple grating patterns reinforce, and reanalysis confirms this: by producing images with a different selection of antenna pairings and/or weighting schemes, the synthesized beam sidelobe structure can in principle be modified such that an array of sources on the sky would produce a less degenerate raw map, but such a combination of antennae was not found. Forthwith, for our analysis we simply consider the A2597 data to comprise a base noise level of 2.9 (4.4) mJy beam^{-1} and an elevated noise level of 10 (15) mJy beam^{-1} in the regime -30 to 0 km s^{-1} for naturally (uniformly) weighted images.

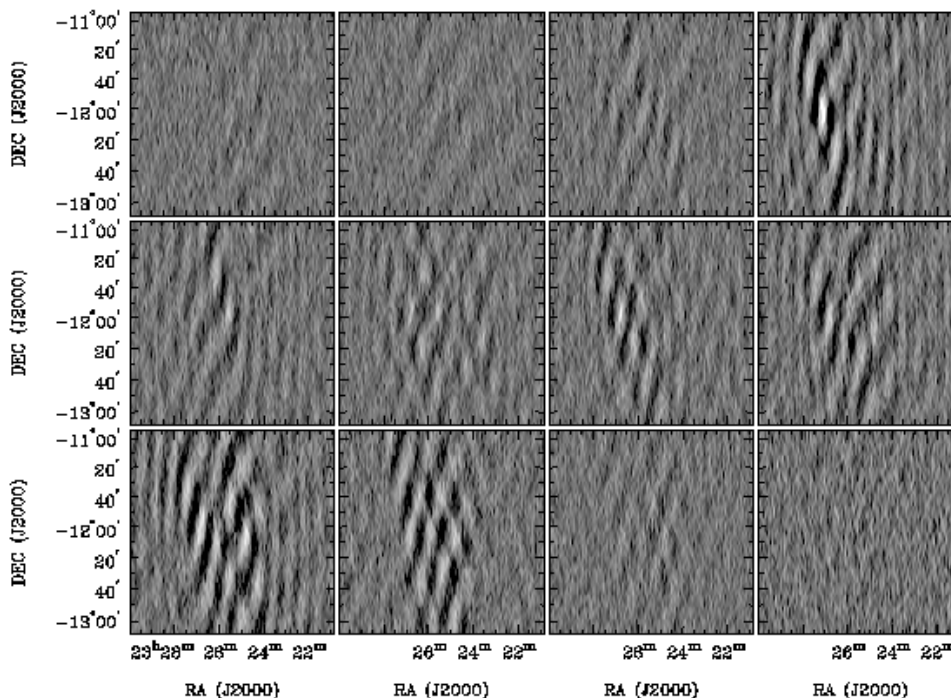


Figure 4. Raw channel maps (ie. unCLEANed) near 0 km s^{-1} for A2597. The greyscale extends from -10 to $+30 \text{ mJy beam}^{-1}$. Sequence is left-to-right, top-to-bottom, with the map at top-left at LSR velocity -33.9 km s^{-1} , and bottom-right $+1.7 \text{ km s}^{-1}$.

3 RESULTS AND DISCUSSION

We calculate upper limits to arcmin scale variations in the foreground neutral hydrogen column density towards the cooling flows in three different ways. The results are listed in Table 2. Columns headed “summed” present the 5σ image noise per channel (as given in Table 1) multiplied by the number of channels in which foreground emission is evident in HI Parkes All Sky Survey spectra² (HIPASS, Barnes et al. 2001), and converted to a column density in the standard way, ie.

$$N_{\text{HI}} = 1.36 \cdot \left(1.823 \times 10^{18}\right) \cdot \frac{\lambda^2}{\theta_a \theta_b} \cdot S_{\text{int}}, \quad (1)$$

where the factor 1.36 incorporates the sensitivity of the ATCA, λ is the observing wavelength (cm), $\theta_{a,b}$ are the major and minor widths of the synthesized observing beam (arcsec, listed in Table 1), S_{int} is the summed flux ($\text{Jy beam}^{-1} \text{ m s}^{-1}$), and the result is in atoms cm^{-2} . Summed limits on beam-to-beam fluctuations in column density are given for both the

² We use HIPASS spectra to estimate the likely spectral extent of the foreground column, as it is a single-dish survey which sees emission at (nearly) all angular scales on the sky.

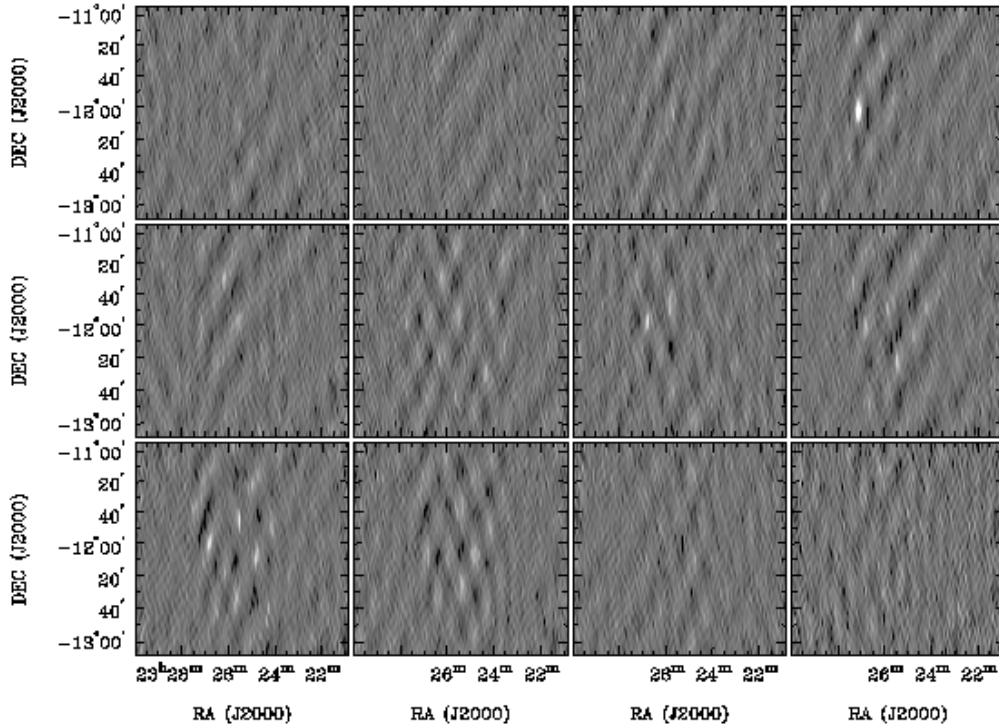


Figure 5. CLEANed channel maps for A2597. Details otherwise identical to Figure 4.

natural and uniform weight maps in Table 2, illustrating the practical trade off between spatial resolution and noise level.

The summed calculation gives a very conservative upper limit to the beam-to-beam fluctuations in N_{H} . These limits apply even if the fluctuation in every channel is in the same sense. However, as noted above, there is little or no correlation from channel to channel in the image slices, so that the contributions of the channels to the noise are largely independent. In this case, the noise in the summed image will be the RMS value for the combined channels. If the channels also contribute equally to the noise, the RMS noise equals the summed noise divided by the square root of the number of channels. Upper limits on foreground column density calculated in this way are given in Table 2 under the heading “averaged.”

Finally, in the columns headed “measured” of Table 2, we list a third set of upper limits to the foreground neutral column density. For each field, we collapse the channel maps by summing those channels for which HIPASS spectra show emission to be present (ie. we generate a zeroth-order moment map) and then calculate the RMS fluctuations in the image plane of the moment map. Importantly, this technique takes into account the channel-to-channel image noise variation, shown in Figures 1–3. In all cases, these “measured” column

density limits lie between the “average” and “summed” values, and we believe them to be the most appropriate limits to use in further analysis.

For comparison with our results, in columns 2 and 3 of Table 2 we list the foreground HI column interpolated from Stark et al. (1992) and Hartmann & Burton (1997) (where available); these data are averaged over beams of area ~ 4.5 and ~ 0.4 square degrees respectively. Our adopted 5σ limits (bold) on the fluctuations in the foreground column are considerably less than the wide-area averaged column itself for the natural weight images (beam areas $\sim 2\text{--}7$ square arcmin), but are on the order of the Stark et al. (1992) column for our uniform weight images (beam areas $\sim 1\text{--}2$ square arcmin). Therefore, our key result is that the foreground HI emission is structureless over the range of scales probed by our natural weighted observations for all three clusters. This outcome is consistent with the extrapolation of the HI power spectra measured at larger angular scales by Green (1993), and with the agreement in HI column measured by the Stark et al. (1992) and Hartmann & Burton (1997) surveys whose beams differ by an order of magnitude in area. Comments on the individual clusters follow.

Abell 3581 is a moderately poor cluster (Postman & Geller 1992) and, perhaps, the least well studied of our objects. Its central galaxy, IC 4374, is a cD galaxy hosting the radio source PKS 1404–267. Based on *ASCA* and *ROSAT* data, Johnstone et al. (1998) found a mass deposition rate of $80 M_{\odot} \text{ yr}^{-1}$, and an absorbing column density of $2 \times 10^{21} \text{ cm}^{-2}$, well in excess of the foreground value (Table 2). Using a redshift of 0.0222 (corresponding to the recession velocity of 6567 km s^{-1} ; Johnstone et al. 1998), the scale is $0.45 \text{ kpc arcsec}^{-1}$, so that our naturally weighted beam size is $62 \times 23 \text{ kpc}$ at the cluster. This is well inside the cooling flow region, which is about 100 kpc in radius (Johnstone et al. 1998). An excess column density of $2 \times 10^{21} \text{ cm}^{-2}$ would violate our 5σ limit if it covered a disc exceeding 5 kpc in radius projected onto the cluster. It is very unlikely that foreground Galactic gas could account for the excess absorption in this object. Our 5σ limit on fluctuations in foreground HI column density from beam-to-beam is about 14 per cent. This constrains the properties of any holes in the foreground gas, as discussed below.

Sersic 159-03, or Abell S1101, has been observed with **XMM-Newton** (Kaastra et al. 2001) and the results show that very little gas cools below $\sim 1 \text{ keV}$. This undermines earlier claims of excess photoelectric absorption in this cluster (Allen & Fabian 1997). At the redshift of the cD galaxy, $z = 0.0564$ (Maia et al. 1987), the cluster scale is $1.1 \text{ kpc arcsec}^{-1}$, so that our naturally weighted beam size is $110 \times 84 \text{ kpc}$. The 5σ limit on fluctuations per

beam in the foreground HI column density is 43 per cent for this cluster. Note that, as discussed in the Introduction, Sersic 159-03 is the cluster with the greatest reported soft X-ray excess (Bonamente et al. 2001).

Abell 2597 has been observed extensively at a wide range of wavelengths. It shares many of the noteworthy properties of cooling flow clusters, including a central radio source, PKS 2322–122 (Sarazin et al. 1995), optical emission lines (Voit & Donahue 1997), recent star formation (Koekemoer et al. 1999) and spatially extended cool gas (Donahue et al. 2000; Edge et al. 2002). Allen et al. (2001) found significant excess photoelectric absorption, but *Chandra* observations show cavities (“ghost” cavities that do not surround the currently detectable radio lobes; McNamara et al. 2000), and that the bulk of the gas does not cool below ~ 1 keV. However, FUSE data do show evidence of some gas cooling to lower temperatures (Oegerle et al. 2001). At a redshift of 0.0821 (Voit & Donahue 1997), the cluster scale is $1.6 \text{ kpc arcsec}^{-1}$, making our naturally weighted beam size $610 \times 91 \text{ kpc}$. Our 5σ limit on the foreground HI fluctuation per beam is 17 per cent for this source.

It is clear that foreground HI emitting gas has little to do with excess photoelectric absorption in any of the three cooling flow clusters considered here. The lack of structure on arcminute scales in any of these clusters tells us that such structure is uncommon at best, at least for sources that are well clear of the Galactic plane.

In the light of the EUV and soft X-ray excesses, for the remainder of this section we focus on placing constraints on holes in the foreground gas (Krick et al. 2000). Our data only place useful constraints on the properties of holes that are comparable in size to the radio beam. For the purpose of discussion, we consider a simple model, with the sky divided into small areas, a , typical of the size of a hole, and smaller than the area A of the radio beam. These areas are covered at random with column density N_0 or $N_1 < N_0$, with the smaller column density to represent holes. If the fraction of the sky covered by holes is f , then the average column density will be $\langle N_{\text{HI}} \rangle = N_0 - f(N_0 - N_1)$. The number of hole areas falling within the radio beam has a binomial distribution, and the RMS fluctuation in the measured column density is $\sigma_N = (N_0 - N_1)\sqrt{f(1-f)a/A}$. The fractional fluctuation in column density from beam-to-beam is then

$$\delta = \frac{\sigma_N}{\langle N_{\text{HI}} \rangle} = \frac{\Delta\sqrt{f(1-f)a/A}}{1-f\Delta},$$

where $\Delta = (N_0 - N_1)/N_0$.

If holes in the foreground HI distribution are to account for EUV and soft X-ray excesses, then the column density in the holes must be significantly lower than average, i.e. we need $\Delta \simeq 1$, so we will take this to be exact. The limits on fluctuations in HI column density from Table 2 may then be regarded as constraining the size of the of any holes, i.e.

$$\sqrt{\frac{a}{A}} < \delta \sqrt{\frac{1-f}{f}},$$

where δ is now the observed limit on the fractional fluctuation in N_{HI} . For example, if the covering fraction of the holes is 1/2, then the constraint is $\sqrt{a/A} < \delta$, giving upper limits to the angular diameter of any holes of 14, 46 and 32 arcsec for Abell 3581, Sersic 159-03 and Abell 2597, respectively, in order to comply with the limits in Table 2. It is unfortunate that our weakest constraint applies to Sersic 159-03, the cluster with the greatest reported soft X-ray excess (Bonamente et al. 2001).

It is interesting to consider what is required of the distribution of the HI gas in order to produce a significant covering fraction of holes. Here, the phrase “low density gas” is used loosely to refer to gas which, if spread along a line of sight, would appear as a significant hole in the foreground HI screen.

The average fraction of a random line of sight that lies in low density gas is equal to the filling factor of that gas. In order to appear as a hole, the bulk of the line of sight must pass through low density gas. Thus, if the covering fraction of holes is substantial, the filling factor of the low density gas needs to be close to unity. The most plausible distribution of HI gas that could appear smooth down to arcmin scales, yet still produce a substantial covering fraction of holes is one where the gas is highly clumped on small scales. The clumps must be significantly smaller than one arcmin in order for the 21 cm emission to appear smooth on that scale. At distances comparable to the gas scale height, ~ 100 pc, a 1 arcmin clump would be ~ 0.03 pc in size. On the other hand, in order to produce appreciable small-scale fluctuations in N_{HI} a typical line of sight can only encounter a small number of clumps. This means that the column density of one clump must be comparable to the mean value of N_{HI} . For small, roughly spherical clumps this requires very high gas densities, $n \gtrsim 10^3 \text{ cm}^{-3}$, almost certainly exceeding the limits on the gas pressure. This constraint is relaxed somewhat if the clumps are really filaments, or folds in sheets (Dickey & Lockman 1990).

Some studies have found variations in foreground HI column density on scales as small as 10 milliarcsec (e.g. Deshpande, Dwarakanath & Goss 2000; Faison & Goss 2001). However,

these variations are seen only in the coldest HI component, and are by no means normal: Faison & Goss (2001) report that only two of seven background continuum sources illuminate opacity gradients in the foreground column. Deshpande (2000) offers a compelling argument that the overall impact on the HI column along different lines of sight from *physically allowable* clouds of cold HI is likely to be very small, and this is again consistent with the studies of the HI power spectrum on larger angular scales (e.g. Green 1993).

4 CONCLUSIONS

Radio maps of the 21 cm emission from foreground Galactic neutral hydrogen over 3 cooling flow clusters show that the gas is uniform on scales from ~ 1 to 10 arcmin. Our 5σ limits on beam-to-beam fluctuations in 21 cm emission, expressed in terms of limits on the fluctuations in HI column density, are 6.2×10^{19} , 7.8×10^{19} and $4.3 \times 10^{19} \text{ cm}^{-2}$ for the clusters Abell 3581, Sersic 159-03 and Abell 2597, respectively, on scales of the order of 1 arcmin (see Table 2). Variations in the column density of neutral hydrogen in the Galaxy do not account for the claimed excess photoelectric absorption in these clusters.

In the light of recent detections of significant excess soft X-ray emission from some clusters, we have also considered whether “holes” in the distribution of foreground neutral hydrogen could cover a significant fraction of the sky, and can confidently rule out a high covering fraction of holes at scales ~ 1 arcmin.

ACKNOWLEDGMENTS

The Australia Telescope is funded by the Commonwealth of Australia for operation as a National Facility managed by the CSIRO. We thank Shane Isley, Mirjam Jonkman and Vincent McIntyre for their help in obtaining the ATCA data. We gratefully acknowledge Lister Staveley-Smith for his advice on reducing the data. We thank Rachel Webster and Martin Meyer for comments on the manuscript. We thank the referee for a thorough and constructive report.

REFERENCES

- Allen S.W., 2000, MNRAS, 315, 269
 Allen S.W., Fabian A.C., 1997, MNRAS, 286, 583

- Allen S.W., Fabian A.C., Johnstone R.M., Arnaud K.A., Nulsen P.E.J., 2001, MNRAS, 322, 589
- Arabadjis J.S., Bregman J.N., 1999, ApJ, 514, 607
- Barnes D.G. et al., 2001, MNRAS, 322, 486
- Berghöfer T.W., Bowyer S., 2002, ApJ, 565, L17
- Blanton E.L., Sarazin C.L., McNamara B.R., Wise M.W., 2001, ApJ, 558, L15
- Bonamente M., Lieu R., Mittaz J.P.D., 2001, ApJ, 561, L63
- Bowyer S., Berghöfer T.W., Korpela E.J., 1999, ApJ, 526, 592
- Churazov E., Sunyaev R., Forman W., Böhringer H., 2002, MNRAS, 332, 729
- Crawford C.S., Allen S.W., Ebeling H., Edge A.C., Fabian A.C., 1999, MNRAS, 306, 857
- David L.P., Jones C., Forman W.R., 1996, ApJ, 473, 692
- David L.P., Nulsen P.E.J., McNamara B.R., Forman W.R., Jones C., Ponman T., Robertson B., Wise M., 2001, ApJ, 557, 546
- Deshpande A.A., 2000, MNRAS, 317, 1999
- Deshpande A.A., Dwarakanath K.S. & Goss W.M., 2000, ApJ, 543, 227
- Dickey J.M. & Lockman F.J., 1990, ARAA, 28, 215
- Donahue M., Mack, J., Voit G.M., Sparks W., Elston R., Maloney P.R., 2000, ApJ, 545, 670
- Edge A.C., 2001, MNRAS, 328, 762
- Edge A.C., Wilman R.J., Johnstone R.M., Crawford C.S., Fabian A.C., Allen S.W., 2002, MNRAS, 337, 49
- Faison M.D. & Goss W.M., 2001, AJ, 121, 2706
- Green D.A., 1993, MNRAS, 262, 327
- Hartmann D., Burton W.B., 1997, Atlas of Galactic Neutral Hydrogen, Cambridge Univ. Press, Cambridge
- Johnstone R.M., Fabian A.C., Nulsen P.E.J., 1987, MNRAS, 224, 75
- Johnstone R.M., Fabian A.C., Taylor G.B., 1998, MNRAS, 298, 854
- Krick J., Arabadjis J.S., Bregman J.N., 2000, BAAS, 197, 07.11
- Fabian A.C., 1994, ARAA, 32, 277
- Fabian A.C., Sanders J.S., Ettori S., Taylor G.B., Allen S.W., Crawford C.S., Iwasawa K., Johnstone R.M., Ogle P.M., 2000, MNRAS, 318, L65
- Fabian A.C., Mushotzky R.F., Nulsen P.E.J. & Peterson J.R., 2001, MNRAS, 321, L20
- Ferland G., Fabian A.C. & Johnstone R.M., 2000, MNRAS, 318, 399

- Jahoda K., McCammon D., Dickey J.M. & Lockman F.J., *ApJ*, 290, 229
- Kaastra J.S., Lieu R., Mittaz J.P.D., Bleeker J.A.M., Mewe R., Colafrancesco S., Lockman F.J., 1999, *ApJ*, 519, L119
- Kaastra J.S., Ferrigno C., Tamura T., Paerels F.B.S., Peterson J.R., Mittaz J.P.D., 2001, *A&A*, 365, L99
- Koekemoer A.M., O’Dea C.P., Sarazin C.L., McNamara B.R., Donahue M., Voit G.M., Baun S.A., Gallimore J.F., 1999, *ApJ*, 525, 621
- Lieu R., Mittaz J.P.D., Bowyer S., Breen J.O., Lockman F.J., Murphy E.M., Hwang C.-Y., 1996, *Science*, 274, 1335
- Maia M.A.G., Da Costa L.N., Willmer C., Pellegrini P.S., Rit  C., 1987, *AJ*, 93, 546
- McNamara B.R., 1997, in Soker N., ed., *Galactic and Cluster Cooling Flows*, Astronomical Society of the Pacific, San Francisco, p. 109
- McNamara B.R., O’Connell R.W., 1992, *ApJ*, 393, 579
- McNamara B.R., Wise M., Nulsen P.E.J., David L.P., Sarazin C.L., Bautz M., Markevitch M., Vikhlinin A., Forman W.R., Jones C., Harris D., 2000, *ApJ*, 534, L135
- Mittaz J.P.D., Kaastra J.S., Tamura T., Fabian A.C., Mushotzky R.F., Peterson J.R., Ikebe Y., Lumb D.H., Paerels F., Stewart G., Trudolyubov S., 2001, *A&A*, 365, L98
- Nulsen P.E.J., David L.P., McNamara B.R., Jones C., Forman W., Wise M., 2002, *ApJ*, 568, 163
- Oegerle W.R., Cowie L., Davidsen A., Hu E., Hutchings J., Murphy E., Sembach K., Woodgate B., 2001, *ApJ*, 560, 187
- Peres C.B., Fabian A.C., Edge A.C., Allen S.W., Johnstone R.M., White D.A., 1998, *MNRAS*, 298, 416
- Peterson J.R., Paerels F.B.S., Kaastra J.S., Arnaud M., Reiprich T.H., Fabian A.C., Mushotzky R.F., Jernigan J.G., Sakelliou I., 2001, *A&A*, 365, L104
- Postman M., Geller M.J., 1992, *ApJ*, 440, 28
- Reynolds J., 1994, “A Revised Flux Scale for the AT Compact Array,” ATNF Internal Report, AT/39.3/040
- Sarazin C.L., Burns J.O., Roettiger K., McNamara B.R., 1995, *ApJ*, 447, 559
- Stark A.A., Gammie C.F., Wilson R.W., Bally J., Linke R.A., Heiles C., Hurwitz M., 1992, *ApJS*, 79, 77
- Tamura T., Kaastra J.S., Peterson J.R., Paerels F.B.S., Mittaz J.P.D., Trudolyubov S.P., Stewart G., Fabian A.C., Mushotzky R.F., Lumb D.H., Ikebe Y., 2001, *A&A*, 365, L87

Voit G.M., Donahue M., 1995, ApJ, 452, 164

Voit G.M., Donahue M., 1997, ApJ, 486, 242

White D.A., Fabian A.C., Johnstone R.M., Mushotzky R.F., Arnaud K., 1991, MNRAS, 252, 72

White D.A., Jones C., Forman W., 1997, MNRAS, 292, 419